Applied Computational Electromagnetics Society

Technical Features

This issue sees the first of a two part feature by Fred Tesche which takes a look at a couple of classic shielding problems.

Electromagnetic Field Shielding of a Spherical Shell – Revisited

Part 1: A Complete Shell

F. M. Tesche
Holcombe Dept. of Electrical and Computer Engineering
College of Engineering & Science, 337 Fluor Daniel Building
Box 340915, Clemson, SC 29634-0915
Fred@Tesche.com

Abstract

This paper takes a fresh look at two classical EM shielding problems involving an integral imperfectly conducting spherical shell and a perfectly conducting hollow sphere with an aperture. Previous studies of the EM shielding provided by these objects have concentrated on evaluating the E- and H-fields at the center of the shield, where only one term of the spherical wave function expansion is needed. While the internal H-field in the shielded volume of the conducting shell is very close to being constant, the same is not true for the E-field, where there can be a significant variation in the E-field intensity from point to point within the interior.

For both of these canonical shielding problems, the method of analysis is described and then applied to determine cumulative probability distributions for the internal fields. In Part 1 of this paper, the frequency-dependent analysis for the case of the complete shell is discussed. To avoid certain numerical overflow problems in evaluating the spherical harmonic solution for lossy media, the use of scaled Hankel functions is described. Additionally, closed-form expressions for the wave expansion coefficients in the spherical coordinate system are derived.

In Part 2 of this paper, the treatment of the hollow sphere with an aperture is obtained using a quasi-static model that also permits the determination of the E-fields anywhere in and around the sphere.

This paper also appears as *Interaction Note 607*, June 5, 2008, Dr. Carl Baum, editor, at www.ece.unm.edu/summa/notes

1. Introduction

There is a continuing need to understand and describe the electromagnetic (EM) field environment inside a protective enclosure that is illuminated by an exterior source. There are several EM standards [1, 2 and 3] that provide measurement procedures to try to obtain shielding effectiveness parameters for enclosures and these standards are often used as requirements for the design and procurement of systems that are protected against external EM fields.

Most of the standards recognize the fact that the EM field within a real enclosure will vary with position and polarization, so that test procedures usually involve making several measurements of the internal field and determining a worst-case shielding estimate. However, due to time and budget constraints, it is unusual to have sufficient measurements to develop a robust statistical representation of the internal fields.

It is possible to use a computational model of an enclosure to determine the internal EM field and its variability. Such models can be of simple canonical shapes like a conducting slab, a cavity bounded by two slabs, a cylinder or a sphere [4, 5]. More complicated models of realistic enclosures having apertures and conducting penetrations are also possible using a finite-difference time domain (FDTD) procedure for solving Maxwell's equations in and around the enclosure [6].

The simplest, yet somewhat realistic, model for shielding is the sphere. Unlike the infinite cylinder or one or more slabs, the sphere has a finite volume, which is typical of a realistic enclosure. Moreover, the EM field in the vicinity of the sphere can be described by relatively simple mathematical functions that permit a numerical computation of the shielding.

Using the spherical wave functions defined by Stratton [7], Harrison and Papas [8] have developed expressions for the E- and H-field at the center of a thin spherical shield due to an incident plane wave excitation. Lindell [9] has examined Harrison's solution near the natural resonances of the sphere, and Shastry [10] has analyzed a hemisphere being excited by a point dipole source. Baum [11] has also examined this problem as a special case illustrating the use of the boundary connection supermatrix (BCS) of a sphere. While all of these investigators have used a modal expansion technique for the solution of the sphere shielding problem, Franceschetti [12] has employed an integral equation method. In each of these references, only the E-fields at the center of the sphere have been considered[1].

---

[1] This may be due to two reasons. First, at the center only the $n = 1$ spherical harmonic is needed, so that evaluating an infinite series summation is not required. Second, it is well-known that the quasi-static magnetic field is constant within the sphere volume, and using the center as the B-field observation point is a good choice. Perhaps it was thought that this location would also be suitable for the E-field. However, as will be shown later, the E-field in the sphere varies significantly with position, and the E-field at the center is significantly lower than the average value of E within the sphere.

Real enclosures have openings, so perhaps a uniform spherical model is not the best one to use for understanding the behavior of the internal fields. References [13, 14, and 15] have described analysis procedures for treating a spherical shell with a circular aperture, but their emphasis is on the scattered EM field, not the internal field distribution. Sancer [16] has described a frequency dependent dual series solution for the internal field in a sphere with a hole, and has used this model to determine the quasi-static E and H-fields. Casey [17] has solved the same problem using a quasi-static dual series model. As in the previous references, only the E-fields at the center of the sphere have been calculated in these latter references. A more general frequency dependent solution for the internal fields in a sphere has been described in [18]. This solution involves a modal expansion for the E-fields and is based on the earlier work of [13]. The emphasis of this work, however, is in the resonance region of the sphere.

The work reported in this paper is a re-visitation of two classical canonical shielding problems: a thin spherical shell made of imperfectly conducting material, which is presented in Part 1, and a perfectly conducting hollow sphere with an aperture, which is discussed in Part 2.

In this Part 1, we describe the analysis of the penetrable sphere by using expansion of spherical vector wave functions in the three regions of the problem: inside and outside the sphere and in the wall material of the sphere. In performing this analysis, closed form expressions for the expansion coefficients are determined and tabulated, and a method for eliminating numerical overflow errors in evaluating the Hankel functions in the wave expansions is described. With a computer program developed to evaluate the E- and H-fields anywhere within the shielded volume of the shell, a Monte Carlo simulation has been performed to generate data suitable for describing the cumulative probability distributions (CPD) for the internal fields.

In Part 2, a quasi-static model useful for computing the internal E-field in a sphere with a hole is reviewed. Because the dual H-field problem can be solved from the E-field solution in this case, only the E-field shielding is discussed here. A Monte Carlo simulation is also performed for this shield, and the corresponding CPDs for the E-field are presented.

2. EM Shielding by a Spherical Shell

In this section, the classical solution for shielding of a spherical shell of imperfectly conducting material is reviewed, and the behavior of the internal and external E and H-fields examined. This solution is essentially the same as described by Harrison [8] and many others, although [8] only provides the expressions for the E-field expansion coefficients for the internal fields. In the development here, we will provide closed-form expressions for the EM field coefficients for all regions. In addition, in the present development we pay special attention to the machine computation of the spherical Hankel functions, which are needed in the solution for the E-fields. In particular, we describe a simple modification of the classical spherical wave expansion functions that permit an accurate evaluation of the E and H-fields inside and outside of the shell.

2.1 Problem Geometry

The geometry of the spherical shell illuminated by an incident plane wave propagating in the z-direction is shown in Figure 1. The incident E-field is taken to be in the *x*-direction, with the H-field being in the *y*-direction. The spherical shell is designated as region #1, and has outer and inner radii of a and b, respectively. The thickness of the shell is denoted by $\Delta = a - b$. The shell is assumed to have the constitutive parameters μ_1 and ε_1 and electrical conductivity σ_1. The material inside and outside the sphere is usually free space and is nonconductive. This material is designated as region #2, with parameters μ_2, ε_2 and $\sigma_2 = 0$. The spherical coordinate system is described by the usual (ρ, θ, ϕ) coordinates, as noted in the figure.

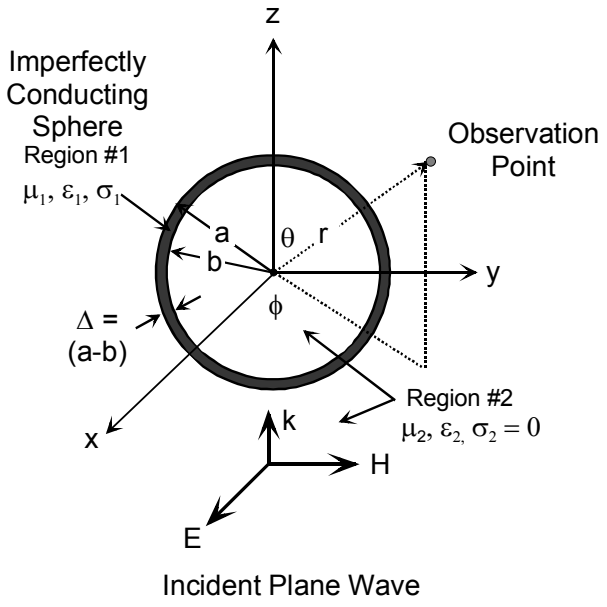

Figure 1. Illustration of a spherical shell illuminated by an incident plane wave.

2.2 Representation of Fields in Spherical Coordinates

In region #1, the wave propagation constant is

$$k_1 \approx \sqrt{\frac{\omega\mu_1\sigma_1}{2}}(1-j) \quad \text{for } \sigma_1 >> \omega\,\varepsilon_1 \tag{1a}$$

and in region #2

$$k_2 = \omega\sqrt{\mu_2\varepsilon_2}\ . \tag{1b}$$

For use later in this paper, the following ratios are defined:

$$\kappa = \frac{k_2}{k_1} \quad \text{and} \quad \Omega = \frac{\mu_2}{\mu_1} \tag{1c}$$

As developed by Stratton [7] (page 414), the EM field in a spherical coordinate system can be expressed as weighted sums of spherical wave vector functions $\overline{m}^{(i)}_{\substack{e\\o}m,n}$ and $\overline{n}^{(i)}_{\substack{e\\o}m,n}$, where indices $n = 0, 1, \cdots \infty$, and $m = 0, 1, \cdots n$. The symbols *e* and *o* denote solutions that are even or odd with respect to the *x* axis, and the index (*i*) denotes the type of radial function used in the expansion. These vector wave functions are expressed as

$$\overline{m}^{(i)}_{\substack{e\\o}m,n} = \mp(-1)^m\, m\, z_n^{(i)}(kr)\frac{P_n^m(\cos\theta)}{\sin\theta}\begin{matrix}\sin\\\cos\end{matrix} m\phi\,\hat{\theta} - (-1)^m\, z_n^{(i)}(kr)\frac{\partial P_n^m(\cos\theta)}{\partial\theta}\begin{matrix}\cos\\\sin\end{matrix} m\phi\,\hat{\phi} \tag{2}$$

$$\begin{aligned}\overline{n}^{(i)}_{\substack{e\\o}m,n} &= n(n+1)(-1)^m\frac{z_n^{(i)}(kr)}{kr}P_n^m(\cos\theta)\begin{matrix}\cos\\\sin\end{matrix} m\phi\,\hat{r}\\ &+(-1)^m\frac{1}{kr}\frac{\partial}{\partial(kr)}\left[kr\, z_n^{(i)}(kr)\right]\frac{\partial P_n^m(\cos\theta)}{\partial\theta}\begin{matrix}\cos\\\sin\end{matrix} m\phi\,\hat{\theta}\\ &\mp(-1)^m\frac{m}{kr\sin\theta}\frac{\partial}{\partial(kr)}\left[kr\, z_n^{(i)}(kr)\right]P_n^m(\cos\theta)\begin{matrix}\sin\\\cos\end{matrix} m\phi\,\hat{\phi}\end{aligned} \tag{3}$$

where the radial function $z_n^{(i)}(kr)$ is

$$z_n^{(i)}(kr) = \begin{bmatrix} j_n(kr) & i=1\\ y_n(kr) & i=2\\ h_n^{(1)}(kr) & i=3\\ h_n^{(2)}(kr) & i=4\end{bmatrix}. \tag{4}$$

and *k* denotes the propagation constant for the specific medium in which the spherical waves are propagating.

The function $P_n^m(x)$ in Eqs.(2) and (3) are the associated Legendre polynomials[2], which according to [19, §8.66] , are defined from the Legendre polynomials $P_n(x)$ by

$$P_n^m(x) = (-1)^m (1-x^2)^{\frac{1}{2}m} \frac{d^m P_n(x)}{dx^m}. \tag{5}$$

From [8] the *x*-directed incident plane wave shown in Figure 1 may be expressed by the spherical wave functions as

$$\begin{aligned} E^i &= E_o e^{-jk_2 x}\hat{x} \\ &= E_o \sum_{n=1}^{\infty} (-j)^n \frac{2n+1}{n(n+1)} \left[\overline{m}_{o,1,n}^{(1)} + j\overline{n}_{e,1,n}^{(1)} \right] \end{aligned} \tag{6a}$$

$$H^i = -\frac{k_2}{\omega\mu_2} E_o \sum_{n=1}^{\infty} (-j)^n \frac{2n+1}{n(n+1)} \left[\overline{m}_{e,1,n}^{(1)} - j\overline{n}_{o,1,n}^{(1)} \right] , \tag{6b}$$

and the scattered (or "reflected") field for $r > a$ is

$$E^r = E_o \sum_{n=1}^{\infty} (-j)^n \frac{2n+1}{n(n+1)} \left[a_n^r \, \overline{m}_{o,1,n}^{(4)} + jb_n^r \overline{n}_{e,1,n}^{(4)} \right] \ (r \geq a) \tag{7a}$$

$$H^r = -\frac{k_2}{\omega\mu_2} E_o \sum_{n=1}^{\infty} (-j)^n \frac{2n+1}{n(n+1)} \left[b_n^r \, \overline{m}_{e,1,n}^{(4)} - ja_n^r \, \overline{n}_{o,1,n}^{(4)} \right] \ (r \geq a). \tag{7b}$$

Note that the arguments of the radial functions in Eqs.(6) and (7) are ($k_2 a$) and the leading factor for the H-field $k_2/\omega\mu_2$ is simply the characteristic wave impedance in medium 2.

Inside the material of the spherical shell, the EM fields are represented in a similar manner, as

---

[2] It is unfortunate that there is an inconsistency in the definition of the associated Legendre polynomials in the literature. Some references, such as Abramowitz [19] include the $(-1)^m$ parameter in the definition, as shown in Eq.(5). However other authors, including Stratton, omit this factor, with the result that the definition of the vector wave functions of Eqs. (3) and (4) can vary from text to text. In this paper, we use Abramowitz's definition and have modified the wave functions of Stratton by adding the term $(-1)^m$ to Eqs. (3) and (4). Butler [20] has surveyed a number of widely used texts for their usage of this term with the following results. Those authors using the $(-1)^m$ term include Abramowitz & Stegun, R. Harrington, D. S. Jones, Magnus & Oberhettinger and S. Schelkunoff. Authors that exclude this term include J. Van Bladel, J. Stratton, A. Sommerfeld and W. Smythe.

$$E^s = E_o \left\{ \begin{array}{l} \displaystyle\sum_{n=1}^{\infty} (-j)^n \frac{2n+1}{n(n+1)} \left[p_n \, \overline{m}_{o,1,n}^{(4)} + j \, q_n \, \overline{n}_{e,1,n}^{(4)} \right] \\ \displaystyle + \sum_{n=1}^{\infty} (-j)^n \frac{2n+1}{n(n+1)} \left[d_n \, \overline{m}_{o,1,n}^{(3)} + j \, f_n \, \overline{n}_{e,1,n}^{(3)} \right] \end{array} \right\} \quad (b < r < a) \tag{8a}$$

$$H^s = -\frac{k_1}{\omega \mu_1} E_o \left\{ \begin{array}{l} \displaystyle\sum_{n=1}^{\infty} (-j)^n \frac{2n+1}{n(n+1)} \left[q_n \, \overline{m}_{e,1,n}^{(4)} - j p_n \, \overline{n}_{o,1,n}^{(4)} \right] \\ \displaystyle + \sum_{n=1}^{\infty} (-j)^n \frac{2n+1}{n(n+1)} \left[f_n \, \overline{m}_{e,1,n}^{(3)} - j d_n \, \overline{n}_{o,1,n}^{(3)} \right] \end{array} \right\} \quad (b < r < a) \tag{8b}$$

with the radial functions arguments being ($k_1 a$).

Inside the sphere void, the E-field representation is

$$E^c = E_o \sum_{n=1}^{\infty} (-j)^n \frac{2n+1}{n(n+1)} \left[a_n^c \, \overline{m}_{o,1,n}^{(1)} + j b_n^c \overline{n}_{e,1,n}^{(1)} \right] \quad (r \le b) \tag{9a}$$

$$H^c = -\frac{k_2}{\omega \mu_2} E_o \sum_{n=1}^{\infty} (-j)^n \frac{2n+1}{n(n+1)} \left[b_n^c \, \overline{m}_{e,1,n}^{(1)} - j a_n^c \, \overline{n}_{o,1,n}^{(1)} \right] \quad (r \le b) \, . \tag{9b}$$

with the radial functions arguments ($k_2 a$).

The eight parameters a_n^r, b_n^r, p_n, q_n, d_n, f_n, a_n^c and b_n^c in Eqs.(7 – 9) are unknowns[3] that can be determined by the boundary conditions at the interfaces at $r = a$ and $r = b$ of the sphere. These boundary conditions are that the tangential components of E and H must be continuous through the interfaces, and are

$$\begin{array}{l} \left(E^i + E^r \right)_\theta = \left(E^s \right)_\theta \quad \text{and} \quad \left(E^i + E^r \right)_\phi = \left(E^s \right)_\phi \\ \left(H^i + H^r \right)_\theta = \left(H^s \right)_\theta \quad \text{and} \quad \left(H^i + H^r \right)_\phi = \left(H^s \right)_\phi \end{array} \quad (\text{at } r = a) \tag{10}$$

and with the same conditions at $r = b$.

In ref. [8], only the $n = 1$ case was considered, as the EM fields were to be calculated only at the center of the sphere. At that location, higher order terms of n in the E-field expansion vanish. For the more general case, however, other values of n must be considered. By applying the boundary conditions independently for each value of n, one can obtain a set of eight equations relating the coefficients $a_n^r, b_n^r \cdots b_n^c$. These equations are

---

[3] These parameters are named in the same way as in ref. [8].

$$j_n(k_2a) + a_n^r h_n^{(2)}(k_2a) = p_n h_n^{(2)}(k_1a) + d_n h_n^{(1)}(k_1a) \tag{11a}$$

$$\left\{ \left[k_2a\, j_n(k_2a) \right]' + b_n^r \left[k_2a\, h_n^{(2)}(k_2a) \right]' \right\} = \kappa \left\{ q_n \left[k_1a\, h_n^{(2)}(k_1a) \right]' + f_n \left[k_1a\, h_n^{(1)}(k_1a) \right]' \right\} \tag{11b}$$

$$\frac{\kappa}{\Omega} \left[j_n(k_2a) + b_n^r h_n^{(2)}(k_2a) \right] = q_n h_n^{(2)}(k_1a) + f_n h_n^{(1)}(k_1a) \tag{11c}$$

$$\frac{1}{\Omega} \left\{ \left[k_2a\, j_n(k_2a) \right]' + a_n^r \left[k_2a\, h_n^{(2)}(k_2a) \right]' \right\} = p_n \left[k_1a\, h_n^{(2)}(k_1a) \right]' + d_n \left[k_1a\, h_n^{(1)}(k_1a) \right]' \tag{11d}$$

$$p_n h_n^{(2)}(k_1b) + d_n h_n^{(1)}(k_1b) = a_n^c\, j_n(k_2b) \tag{11e}$$

$$\kappa \left\{ q_n \left[k_1b\, h_n^{(2)}(k_1b) \right]' + f_n \left[k_1b\, h_n^{(1)}(k_1b) \right]' \right\} = b_n^c \left[k_2b\, j_n(k_2b) \right]' \tag{11f}$$

$$\frac{\Omega}{\kappa} \left[q_n h_n^{(2)}(k_1b) + f_n h_n^{(1)}(k_1b) \right] = b_n j_n(k_2b) \tag{11g}$$

$$\Omega \left\{ p_n \left[k_1b\, h_n^{(2)}(k_1b) \right]' + d_n \left[k_1b\, h_n^{(1)}(k_1b) \right]' \right\} = a_n^c \left[k_2b\, j_n(k_2b) \right]' \tag{11h}$$

where the parameters κ and Ω have been defined in Eq.(1c).

2.3 Scaling of the Hankel Functions and Expansion Coefficients

In trying to use these equations for determining the expansion coefficients, there is a problem that arises in the evaluation of the wave functions in region #1 where $k = k_1$, due to the exponential variation of the Hankel functions $h_n^{(1)}(ka)$ and $h_n^{(1)}(kb)$. To see this, ref[19, §10.1.16] provides the following representations for the spherical Hankel functions

$$\begin{aligned} h_n^{(1)}(kr) &= j^{-n-1}(kr)^{-1} e^{jkr} \sum_{k=0}^{n} \frac{(n+k)!}{k!\Gamma(n-k+1)} (-2jkr)^{-k} \\ &\equiv e^{jkr} \hat{h}_n^{(1)}(kr) \end{aligned} \tag{12a}$$

$$\begin{aligned} h_n^{(2)}(kr) &= j^{n+1}(kr)^{-1} e^{-jkr} \sum_{k=0}^{n} \frac{(n+k)!}{k!\Gamma(n-k+1)} (2jkr)^{-k} \\ &\equiv e^{-jkr} \hat{h}_n^{(2)}(kr) \end{aligned} \tag{12b}$$

These relationships define $\hat{h}_n^{(1)}(kr)$ and $\hat{h}_n^{(2)}(kr)$, which are *scaled Hankel functions*[4]. These scaled functions maintain reasonable accuracy over a wide range of the complex parameter (*kr*) and are provided by many special function routines. Note that this is not an approximation to the Hankel functions, but rather, just a factorization of the functions.

As a consequence of Eq.(12a), we observe that in region #1 $h_n^{(1)}(kr) \sim e^{\sqrt{\frac{\omega\mu_1\sigma_1}{2}}r}$ and this function becomes unbounded as $\omega \to \infty$. The direct use of this function in a numerical calculation becomes impossible at high frequencies – even if its exponential growth may be ultimately cancelled somewhere in a complicated expression by the exponential decrease of functions like $h_n^{(2)}(kr) \sim e^{-\sqrt{\frac{\omega\mu_1\sigma_1}{2}}r}$.

To solve this problem, we express the boundary conditions and Hankel functions in region #1 using the scaled spherical Hankel functions and the appropriate scaling factors as

$$h_n^{(1)}(k_1 a) = T_1 \hat{h}_n^{(1)}(k_1 a) \qquad h_n^{(2)}(k_1 a) = \frac{1}{T_1}\hat{h}_n^{(2)}(k_1 a) \tag{13}$$

$$h_n^{(1)}(k_1 b) = \frac{T_1}{T_\Delta}\hat{h}_n^{(1)}(k_1 b) \qquad h_n^{(2)}(k_1 b) = \frac{T_\Delta}{T_1}\hat{h}_n^{(2)}(k_1 b) \tag{14}$$

where $T_1 = e^{jk_1 a}$ and $T_\Delta = e^{jk_1(a-b)} = e^{jk_1\Delta}$.

Using these scaled Hankel functions in region #1, the boundary conditions in Eqs.(11) can be written in a compact matrix form as

[4] In this paper, any parameter or function with the ^ symbol is designated as a scaled quantity.

$$
\begin{bmatrix}
-h_n^{(2)}(k_2a) & 0 & \frac{1}{T_1}\hat{h}_n^{(2)}(k_1a) & 0 & T_1\hat{h}_n^{(1)}(k_1a) & 0 & 0 & 0 \\
0 & -\left[k_2a\,h_n^{(2)}(k_2a)\right]' & 0 & \frac{\kappa}{T_1}\left[k_1a\,\hat{h}_n^{(2)}(k_1a)\right]' & 0 & \kappa T_1\left[k_1a\,\hat{h}_n^{(1)}(k_1a)\right]' & 0 & 0 \\
0 & -\frac{\kappa}{\Omega}h_n^{(2)}(k_2a) & 0 & \frac{1}{T_1}\hat{h}_n^{(2)}(k_1a) & 0 & T_1\,\hat{h}_n^{(1)}(k_1a) & 0 & 0 \\
-\frac{1}{\Omega}\left[k_2a\,h_n^{(2)}(k_2a)\right]' & 0 & \frac{1}{T_1}\left[k_1a\hat{h}_n^{(2)}(k_1a)\right]' & 0 & T_1\left[k_1a\hat{h}_n^{(1)}(k_1a)\right]' & 0 & 0 & 0 \\
0 & 0 & \frac{T_\Delta}{T_1}\hat{h}_n^{(2)}(k_1b) & 0 & \frac{T_\Delta}{T_\Delta}\hat{h}_n^{(1)}(k_1b) & 0 & -j_n(k_2b) & 0 \\
0 & 0 & 0 & \frac{T_\Delta}{T_1}\kappa\left[k_1b\hat{h}_n^{(2)}(k_1b)\right] & 0 & \frac{T_1}{T_\Delta}\kappa\left[k_1b\hat{h}_n^{(1)}(k_1b)\right]' & 0 & -\left[k_2b\,j_n(k_2b)\right]' \\
0 & 0 & 0 & \frac{T_\Delta}{T_1}\frac{\Omega}{\kappa}\hat{h}_n^{(2)}(k_1b) & 0 & \frac{T_1}{T_\Delta}\frac{\Omega}{\kappa}\hat{h}_n^{(1)}(k_1b) & 0 & -j_n(k_2b) \\
0 & 0 & \frac{T_\Delta}{T_1}\Omega\left[k_1b\hat{h}_n^{(2)}(k_1b)\right]' & 0 & \frac{T_1}{T_\Delta}\Omega\left[k_1b\hat{h}_n^{(1)}(k_1b)\right]' & 0 & -\left[k_2b\,j_n(k_2b)\right]' & 0
\end{bmatrix}
\begin{bmatrix}
a_n' \\ b_n' \\ p_n \\ q_n \\ d_n \\ f_n \\ a_n^c \\ b_n^c
\end{bmatrix}
=
\begin{bmatrix}
j_n(k_2a) \\ \left[k_2a\,j_n(k_2a)\right]' \\ \frac{\kappa}{\Omega}j_n(k_2a) \\ \frac{1}{\Omega}\left[k_2a\,j_n(k_2a)\right]' \\ 0 \\ 0 \\ 0 \\ 0
\end{bmatrix}
\tag{15}
$$

To observe the effects of using the scaled Hankel functions and to provide an alternative to a strict numerical inversion of Eq.(15), it is useful to develop closed-form expressions for the expansion coefficients. Reference [8] provides expressions for the coefficients a_1^c and b_1^c for the E-fields at the center of the sphere, and here we generalize their results for arbitrary n and for all regions. It should also be mentioned that Baum [11] in his Appendix A also provides expressions for the expansion coefficients, but not in stand-alone terms, but as ratios of confidents, relative to the coefficients of the incident plane wave.

Obtaining such a symbolic solution is tedious but it can be accomplished using a symbolic solver to invert Eq.(15) and obtain algebraic expressions for the coefficients. In doing this there are two terms that occur in the denominators of the various expressions for the coefficients. These are denoted as *Den1* and *Den2* and are

$$\begin{aligned} Den1_n = \frac{1}{T_\Delta}\Big[&\Big(\Omega\, j_n(k_2b)\big[k_1b\,\hat{h}_n^{(1)}(k_1b)\big]' - \big[k_2b\, j_n(k_2b)\big]'\,\hat{h}_n^{(1)}(k_1b)\Big)\Big(\hat{h}_n^{(2)}(k_1a)\big[k_2a\,h_n^{(2)}(k_2a)\big]' - \Omega\, h_n^{(2)}(k_2a)\big[k_1a\,\hat{h}_n^{(2)}(k_1a)\big]'\Big)\Big] \\ &+T_\Delta\Big[\Big(\Omega\, j_n(k_2b)\big[k_1b\,\hat{h}_n^{(2)}(k_1b)\big]' - \big[k_2b\, j_n(k_2b)\big]'\,\hat{h}_n^{(2)}(k_1b)\Big)\Big(\Omega\, h_n^{(2)}(k_2a)\big[k_1a\,\hat{h}_n^{(1)}(k_1a)\big]' - \hat{h}_n^{(1)}(k_1a)\big[k_2a\,h_n^{(2)}(k_2a)\big]'\Big)\Big] \end{aligned} \quad (16a)$$

$$\begin{aligned} Den2_n = \frac{1}{T_\Delta}\Big[&\Big(\kappa^2 j_n(k_2b)\big[k_1b\,\hat{h}_n^{(1)}(k_1b)\big]' - \Omega\big[k_2b\, j_n(k_2b)\big]'\,\hat{h}_n^{(1)}(k_1b)\Big)\Big(\Omega\,\hat{h}_n^{(2)}(k_1a)\big[k_2a\,h_n^{(1)}(k_2a)\big]' - \kappa^2\, h_n^{(2)}(k_2a)\big[k_1a\,\hat{h}_n^{(2)}(k_1a)\big]'\Big)\Big] \\ &+T_\Delta\Big[\Big(\kappa^2 j_n(k_2b)\big[k_1b\,\hat{h}_n^{(2)}(k_1b)\big]' - \Omega\big[k_2b\, j_n(k_2b)\big]'\,\hat{h}_n^{(2)}(k_1b)\Big)\Big(\kappa^2\, h_n^{(2)}(k_2a)\big[k_1a\,\hat{h}_n^{(1)}(k_1a)\big]' - \Omega\,\hat{h}_n^{(1)}(k_1a)\big[k_2a\,h_n^{(2)}(k_2a)\big]'\Big)\Big] \end{aligned} \quad (16b)$$

It is important to note that the scaling function T_1 does not occur in these denominator functions as they have cancelled out in the products of terms like $\hat{h}_n^{(1)}(k_1b)\cdot\hat{h}_n^{(2)}(k_1a)$. There still is the scaling function $T_\Delta = e^{jk_1\Delta}$ present in these expressions, but for thin shells, this term is easily computed and it does not become so large as to cause numerical round-off problems.

The unscaled parameters a_n^r, b_n^r, p_n, q_n, d_n, f_n, a_n^c and b_n^c are given in closed form as follows:

$$\begin{aligned} a_n^r = -\frac{1}{Den1_n}\frac{1}{T_\Delta}&\Big[\Big(\hat{h}_n^{(2)}(k_1a)\big[k_2a\, j_n(k_2a)\big]' - \Omega\, j_n(k_2a)\big[k_1a\,\hat{h}_n^{(2)}(k_1a)\big]'\Big)\Big(\Omega\, j_n(k_2b)\big[k_1b\,\hat{h}_n^{(1)}(k_1b)\big]' - \hat{h}_n^{(1)}(k_1b)\big[k_2b\, j_n(k_2b)\big]'\Big)\Big] \\ -\frac{1}{Den1_n}T_\Delta&\Big[\Big(\hat{h}_n^{(1)}(k_1a)\big[k_2a\, j_n(k_2a)\big]' - \Omega\, j_n(k_2a)\big[k_1a\,\hat{h}_n^{(1)}(k_1a)\big]'\Big)\Big(\hat{h}_n^{(2)}(k_1b)\big[k_2b\, j_n(k_2b)\big]' - \Omega\, j_n(k_2b)\big[k_1b\,\hat{h}_n^{(2)}(k_1b)\big]'\Big)\Big] \end{aligned} \quad (17a)$$

$$\begin{aligned} b_n^r = -\frac{1}{Den2_n}\frac{1}{T_\Delta}&\Big[\Big(\Omega\,\hat{h}_n^{(2)}(k_1a)\big[k_2a\, j_n(k_2a)\big]' - \kappa^2 j_n(k_2a)\big[k_1a\,\hat{h}_n^{(2)}(k_1a)\big]'\Big)\Big(\kappa^2 j_n(k_2b)\big[k_1b\,\hat{h}_n^{(1)}(k_1b)\big]' - \Omega\,\hat{h}_n^{(1)}(k_1b)\big[k_2b\, j_n(k_2b)\big]'\Big)\Big] \\ -\frac{1}{Den2_n}T_\Delta&\Big[\Big(\kappa^2 j_n(k_2a)\big[k_1a\,\hat{h}_n^{(1)}(k_1a)\big]' - \Omega\,\hat{h}_n^{(1)}(k_1a)\big[k_2a\, j_n(k_2a)\big]'\Big)\Big(\kappa^2 j_n(k_2b)\big[k_1b\,\hat{h}_n^{(2)}(k_1b)\big]' - \Omega\,\hat{h}_n^{(2)}(k_1b)\big[k_2b\, j_n(k_2b)\big]'\Big)\Big] \end{aligned} \quad (17b)$$

$$p_n = -\frac{1}{Den1_n}\frac{T_1}{T_\Delta}\left[\left(\frac{-j}{k_2 a}\right)\left(\hat{h}_n^{(1)}(k_1 b)\left[k_2 b\, j_n(k_2 b)\right]' - \Omega\, j_n(k_2 b)\left[k_1 b\, \hat{h}_n^{(1)}(k_1 b)\right]'\right)\right] \tag{17c}$$

$$q_n = -\frac{\kappa}{Den2_n}\frac{T_1}{T_\Delta}\left[\left(\frac{-j}{k_2 a}\right)\left(\Omega\, \hat{h}_n^{(1)}(k_1 b)\left[k_2 b\, j_n(k_2 b)\right]' - \kappa^2\, j_n(k_2 b)\left[k_1 b\, \hat{h}_n^{(1)}(k_1 b)\right]'\right)\right] \tag{17d}$$

$$d_n = \frac{1}{Den1_n}\frac{T_\Delta}{T_1}\left[\left(\frac{-j}{k_2 a}\right)\left(\hat{h}_n^{(2)}(k_1 b)\left[k_2 b\, j_n(k_2 b)\right]' - \Omega\, j_n(k_2 b)\left[k_1 b\, \hat{h}_n^{(2)}(k_1 b)\right]'\right)\right] \tag{17e}$$

$$f_n = \frac{\kappa}{Den2_n}\frac{T_\Delta}{T_1}\left[\left(\frac{-j}{k_2 a}\right)\left(\Omega\, \hat{h}_n^{(2)}(k_1 b)\left[k_2 b\, j_n(k_2 b)\right]' - \kappa^2\, j_n(k_2 b)\left[k_1 b\, \hat{h}_n^{(2)}(k_1 b)\right]'\right)\right] \tag{17f}$$

$$a_n^c = \frac{\Omega}{Den1_n}\left(\frac{-j}{k_2 a}\right)\left(\frac{2j}{k_1 b}\right) \tag{17g}$$

$$b_n^c = \frac{\Omega\kappa^2}{Den2_n}\left(\frac{-j}{k_2 a}\right)\left(\frac{2j}{k_1 b}\right) \tag{17h}$$

Equations (17c) through (17h) have been simplified somewhat through the use of appropriate Wronskian relationships between the radial functions. Reference [11] also discusses this simplification. Furthermore, if $\Omega = 1$, additional simplifications are possible.

Notice that in Eqs.(17a, b, g and f) for parameters a_n^r, b_n^r, a_n^c and b_n^c the scaling factors T_1 and $1/T_1$ have all canceled with each other, and these parameters do not occur in the solution. The evaluation of these parameters using the scaled Hankel functions poses no problem at all. However, if Eq.(16) were to be solved numerically, there would be serious overflow and underflow problems due to the presence of the scaling factors.

Furthermore, in Eqs.(17) we observe that the parameters p_n and q_n are proportional to T_1, and parameters d_n and f_n are proportional to $1/T_1$. These expressions show symbolically why the direct evaluation of even these closed-form coefficients is prone to error due to the very large or very small values of these proportionality constants. By removing the T_1 scaling parameter from Eqs.(17c) – (17f) as

$$\begin{aligned} p_n &= T_1 \hat{p}_n \qquad q_n = T_1 \hat{q}_n \\ d_n &= \frac{1}{T_1}\hat{d}_n \qquad f_n = \frac{1}{T_1}\hat{f}_n \end{aligned} \tag{18}$$

we can define *scaled* expansion parameters $\hat{p}_n$, $\hat{q}_n$, $\hat{d}_n$, $\hat{f}_n$, which are

$$\hat{p}_n = -\frac{1}{Den1_n}\frac{1}{T_\Delta}\left[\left(\frac{-j}{k_2 a}\right)\left(\hat{h}_n^{(1)}(k_1 b)\left[k_2 b\, j_n(k_2 b)\right]' - \Omega\, j_n(k_2 b)\left[k_1 b\, \hat{h}_n^{(1)}(k_1 b)\right]'\right)\right] \quad (19a)$$

$$\hat{q}_n = -\frac{\kappa}{Den2_n}\frac{1}{T_\Delta}\left[\left(\frac{-j}{k_2 a}\right)\left(\Omega\, \hat{h}_n^{(1)}(k_1 b)\left[k_2 b\, j_n(k_2 b)\right]' - \kappa^2 j_n(k_2 b)\left[k_1 b\, \hat{h}_n^{(1)}(k_1 b)\right]'\right)\right] \quad (19b)$$

$$\hat{d}_n = \frac{1}{Den1_n} T_\Delta\left[\left(\frac{-j}{k_2 a}\right)\left(\hat{h}_n^{(2)}(k_1 b)\left[k_2 b\, j_n(k_2 b)\right]' - \Omega\, j_n(k_2 b)\left[k_1 b\, \hat{h}_n^{(2)}(k_1 b)\right]'\right)\right] \quad (19c)$$

$$\hat{f}_n = \frac{\kappa}{Den2_n} T_\Delta\left[\left(\frac{-j}{k_2 a}\right)\left(\Omega\, \hat{h}_n^{(2)}(k_1 b)\left[k_2 b\, j_n(k_2 b)\right]' - \kappa^2 j_n(k_2 b)\left[k_1 b\, \hat{h}_n^{(2)}(k_1 b)\right]'\right)\right] \quad (19d)$$

The use of these scaled parameters in evaluating the E- and H-fields is discussed in the next section.

It is worth pointing out that the evaluation of the required set of unscaled parameters a_n^r, b_n^r, a_n^c and b_n^c and scaled parameters $\hat{p}_n$, $\hat{q}_n$, $\hat{d}_n$, $\hat{f}_n$ can also be computed from a numerical inversion of Eq.(15). This may be done by setting the scaling parameter T_1 = 1 and using scaled Hankel functions $\hat{h}_n^{(1)}(k_1 a)$, $\hat{h}_n^{(2)}(k_1 a)$, $\hat{h}_n^{(1)}(k_1 b)$ and $\hat{h}_n^{(2)}(k_1 b)$ as indicated in Eq.(15) to obtain a numerically stable matrix equation that can be easily inverted. Although there is not much insight into the structure of the solution for these parameters in this numerical approach, the coding of this equation is certainly much simpler (and less error-prone) than developing code for the closed-form expressions.

2.4 Use of Scaled Parameters in Determining E- and H-fields

To use these scaled coefficients in the solution for the E-fields in the sphere, we observe that in Eq.(8) the p_n and q_n parameters are always multiplied by $h_n^{(2)}(k_1 r)$ and d_n and f_n occur together with $h_n^{(1)}(k_1 r)$. Thus, in Eq.(8) the product $p_n\, \overline{m}_{o,1,n}^{(4)}$ can be written as

$$p_n\, \overline{m}_{o,1,n}^{(4)} = T_1 \hat{p}_n\, e^{-jk_1 r}\, \hat{\overline{m}}_{o,1,n}^{(4)} \quad (20)$$

where the exponential scaling factor $e^{-jk_1 r}$ has been extracted from the Hankel function $h_n^{(2)}(k_1 r)$. The term $\hat{\overline{m}}_{o,1,n}^{(4)}$ denotes the spherical harmonic function *evaluated with the scaled Hankel function* $\hat{h}_n^{(2)}(k_1 r)$.

The scaling terms in Eq.(20) can be combined into a common factor $S(k_1 r)$ as

$$p_n\,\bar{m}^{(4)}_{o,1,n} = S\left(k_1 r\right)\hat{p}_n\,\hat{\bar{m}}^{(4)}_{o,1,n} \tag{21}$$

with

$$S\left(k_1 r\right) \equiv e^{\,jk_1(a-r)}\,. \tag{22}$$

Similarily, the other products of the parameters and wave functions can be written as

$$q_n\,\bar{m}^{(4)}_{e,1,n} = S\left(k_1 r\right)\hat{q}_n\,\hat{\bar{m}}^{(4)}_{e,1,n} \qquad p_n\,\bar{n}^{(4)}_{o,1,n} = S\left(k_1 r\right)\hat{p}_n\,\hat{\bar{n}}^{(4)}_{o,1,n} \qquad q_n\,\bar{n}^{(4)}_{e,1,n} = S\left(k_1 r\right)\hat{q}_n\,\hat{\bar{n}}^{(4)}_{e,1,n} \tag{23}$$

The other terms in the expression involving d_n and f_n are of the form

$$\begin{aligned} d_n\,\bar{m}^{(3)}_{o,1,n} &= \frac{1}{S\left(k_1 r\right)}\hat{d}_n\,\hat{\bar{m}}^{(3)}_{o,1,n} \qquad & f_n\,\bar{m}^{(3)}_{e,1,n} &= \frac{1}{S\left(k_1 r\right)}\hat{f}_n\,\hat{\bar{m}}^{(3)}_{e,1,n} \\ d_n\,\bar{n}^{(3)}_{o,1,n} &= \frac{1}{S\left(k_1 r\right)}\hat{d}_n\,\hat{\bar{n}}^{(3)}_{o,1,n} \qquad & f_n\,\bar{n}^{(3)}_{e,1,n} &= \frac{1}{S\left(k_1 r\right)}\hat{f}_n\,\hat{\bar{n}}^{(3)}_{e,1,n} \end{aligned} \tag{24}$$

Thus, in region #1 where $b < r < a$, the E and H-fields are expressed using a relationship similar to that of Eq.(8), but with the *scaled* expansion coefficients and Hankel functions *and* the scaling factor S:

$$E^s = E_o\left\{\begin{aligned}&\sum_{n=1}^{\infty}(-j)^n\,\frac{2n+1}{n(n+1)}\,S\left(k_1 r\right)\left[\,\hat{p}_n\,\hat{\bar{m}}^{(4)}_{o,1,n} + j\,\hat{q}_n\,\hat{\bar{n}}^{(4)}_{e,1,n}\,\right] \\ &+\sum_{n=1}^{\infty}(-j)^n\,\frac{2n+1}{n(n+1)}\,\frac{1}{S\left(k_1 r\right)}\left[\,\hat{d}_n\,\hat{\bar{m}}^{(3)}_{o,1,n} + j\,\hat{f}_n\,\hat{\bar{n}}^{(3)}_{e,1,n}\,\right]\end{aligned}\right\} \quad (b < r < a) \tag{25a}$$

$$H^s = -\frac{k_1}{\omega\mu_1}E_o\left\{\begin{aligned}&\sum_{n=1}^{\infty}(-j)^n\,\frac{2n+1}{n(n+1)}\,S\left(k_1 r\right)\left[\,\hat{q}_n\,\hat{\bar{m}}^{(4)}_{e,1,n} - j\hat{p}_n\,\hat{\bar{n}}^{(4)}_{o,1,n}\,\right] \\ &+\sum_{n=1}^{\infty}(-j)^n\,\frac{2n+1}{n(n+1)}\,\frac{1}{S\left(k_1 r\right)}\left[\,\hat{f}_n\,\hat{\bar{m}}^{(3)}_{e,1,n} - j\hat{d}_n\,\hat{\bar{n}}^{(3)}_{o,1,n}\,\right]\end{aligned}\right\} \quad (b < r < a) \tag{25b}$$

This scaling procedure permits the computation of the E-fields over a broad frequency range, which is impossible with the conventional wave expansion of Eq.(8). For the E-fields in the other regions where $r > a$ and $r < b$, the unscaled expressions in Eqs. (6), (7) and (9) can be used.

2.5 Numerical Results

A computer program was developed to evaluate Eqs. (6), (7), (9) and (25) using the closed form expressions for the expansion coefficients. As a check of this solution, it was verified that the various boundary conditions on the sphere were met, and that the overall behavior of the E-fields was correct.

As an additional check, the E-field and H-field transfer functions at the center of an aluminum shell (σ = 3.54 x 10^7 S/m) with radius a = 0.914 m (36 in) and thicknesses Δ = 0.794, 1.587 and 3.175 mm (corresponding to 1/32, 1/16 and 1/8 inches) were computed. This sphere is the same as that used in [8]. For these comparisons, transfer functions relating the total E and H-field magnitudes to the magnitude of the incident E-field are defined as

$$TE(r,\theta,\phi) = \frac{\left|\vec{E}(r,\theta,\phi)\right|}{E_o} \quad and \quad TH(r,\theta,\phi) = \frac{\left|\vec{H}(r,\theta,\phi)\right|}{E_o} \tag{26}$$

In Eq.(26), the transfer function TE is unitless and TH has units of Siemens, which is not ideal, but this is done to permit a direct comparison with the results of [8]. Figure 2 presents plots of the E-field and H-field transfer functions, expressed in dB, at the center of the aluminum sphere with different shell thicknesses, Δ. These plots are identical with those in Figures 2 and 8 of ref. [8], and this serves as a partial validation of the computational procedure. Note that usually the H-field transfer function is shown relative to the incident H-field, not the E-field, and at low frequencies, $H/H_o \rightarrow 0$ dB. The low frequency limit in Figure 2a is –51.53 dB, which is exactly $1/Z_o$ expressed in dB.

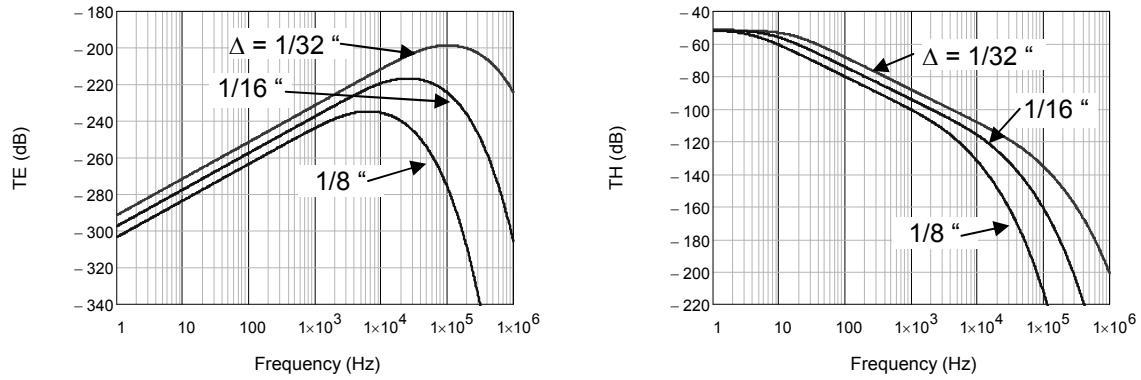

a. E-field transfer function b. H-field transfer function

Figure 2. Plots of the total E-field and H-field transfer functions at the center of an aluminum sphere with radius a = 0.914 m for different shell thicknesses, Δ. (To be compared with Figures 2 and 8 of ref. [8].)

It is interesting to see that the upper frequency response of the transfer functions in Figure 2 is 1 MHz. Even for this relatively low frequency, the spherical wave function series is difficult to evaluate without scaling the Hankel functions. To illustrate the robustness of the

present scaled solution at higher frequencies, Figure 3a presents a plot of the E-field transfer functions for the sphere for frequencies up to 1 GHz. The responses are reasonable in appearance, and if one carefully examines the transfer function for the thinnest shell, a hint of small peaks in the curves are seen at frequencies above about 200 MHz. Figure 3b plots the transfer function for this shell on a linear scale and these peaks are seen more clearly.

These peaks are due to the internal resonances in the shell. Since the shell material is highly conducting, we expect that these resonances will occur close to the classical internal resonances of a perfectly conducting sphere. According to Harrington [21, §6-2], such internal resonances occur at the roots of $J_n(k_2 b) = 0$ for the TE modes, and at the roots of $[k_2 b\, J_n(k_2 b)]' = 0$ for the TM modes. Table 1. presents the roots for the first four TM modes, along with the resulting resonant frequencies for the sphere with a radius of about 0.914 m. We see that the agreement with the frequencies of the resonances in Figure 3b is very good. Of course, since the conductivity of the shell is so high, the internal E-field is extremely small – 1000 to 2000 dB down from the incident field.

Table 1. Interior TM resonances for a perfectly conducting shell.

No.	$k_2 b$	Freq. (GHz)
1	2.744	0.143
2	6.117	0.320
3	9.317	0.487
4	12.486	0.653

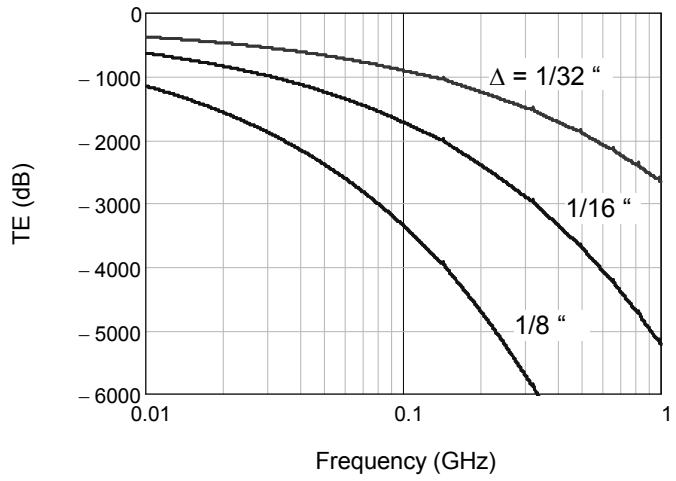

a. TE for three different shell thicknesses.

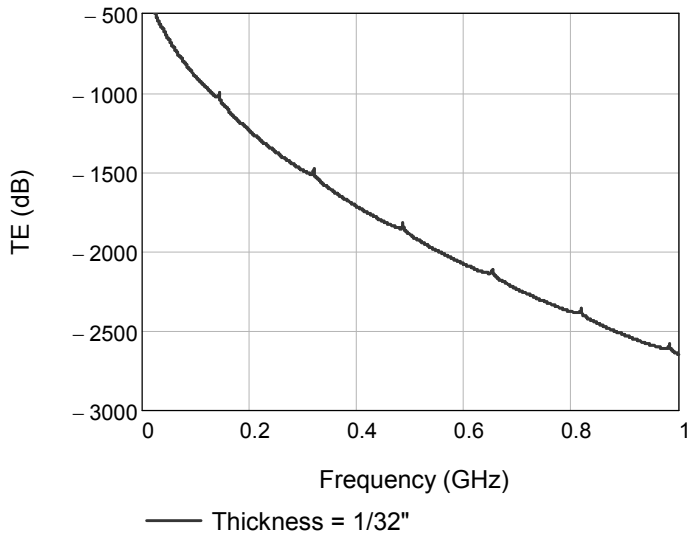

b. Linear plot of TE for a shell of thickness Δ = 1/32 in.

Figure 3. Plots of the total E-field transfer function at the center of the spherical shell for higher frequencies up to 1 GHz.

The primary motive for this study is to understand the behavior of the internal E- and H-fields within the shell. Using the same spherical shell as in the previous example, the transfer functions for the individual components of the E- and H-fields have been evaluated along the radial path in the direction defined by the angles $\theta = 90^o$ and $\phi = 45^o$. With reference to Figure 1, this path is in the *x*-*y* plane at $z = 0$ and at an angle of 45^o to the *x* axis. Figure 4 shows these E-fields as a function of normalized radial distance *r*/*b* from the origin to *r*/*b* = 2 for a frequency of $f = 100$ kHz.

The important thing to observe from this plot is that for both the E- and H-fields inside the shell, there are observable spatial variations in the E-field components. For the H-field, the H_r and H_θ components are equal in magnitude (on this particular radial trajectory), but there is a definite variation of the H_ϕ component. For the E-field, the principal component is E_θ and its spatial variation is significant. Outside the sphere both the E- and H-fields approach the incident field at distances of $r/b \approx 2$.

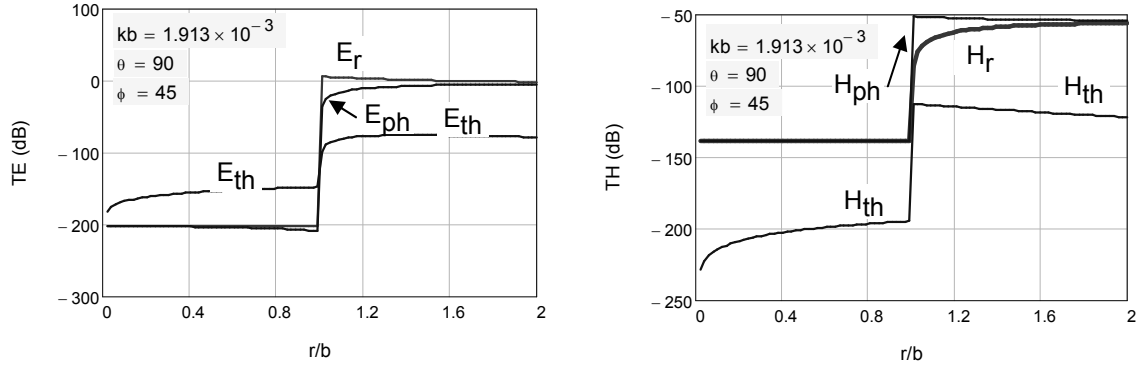

a. Electric field b. Magnetic field

Figure 4. E- and H-field transfer functions for the *r*, θ and ϕ field components for the spherical shell of inner radius *b* = 0.914 m and shell thickness Δ = 0.794 mm, at a frequency of 100 kHz. (These E-fields are shown as a function of radial distance on a path defined by the angles $\theta = 90^o$ and $\phi = 45^o$.)

Perhaps a more intuitive measure of the internal shell fields is the total field transfer functions given by Eq.(26). Figure 5 illustrates the behavior of the E-field transfer functions in the equatorial ($z = 0$) plane along different trajectories defined by the angle ϕ. Parameters are the same as in the previous example: $b = 0.914$ m, $\Delta = 0.794$ mm, and $f = 100$ kHz.

In this figure, it is clear that the total internal H-field in the shell is constant for all practical purposes. However, there can be a significant variation of the total E-field inside the shell – about 60 dB, or a factor of 1000. Furthermore, we see that the value of TE for this shield reported in ref. [8] (at the center of the shell) is about – 198 dB. This is clearly not a representative measure of the shielding provided by this shell.

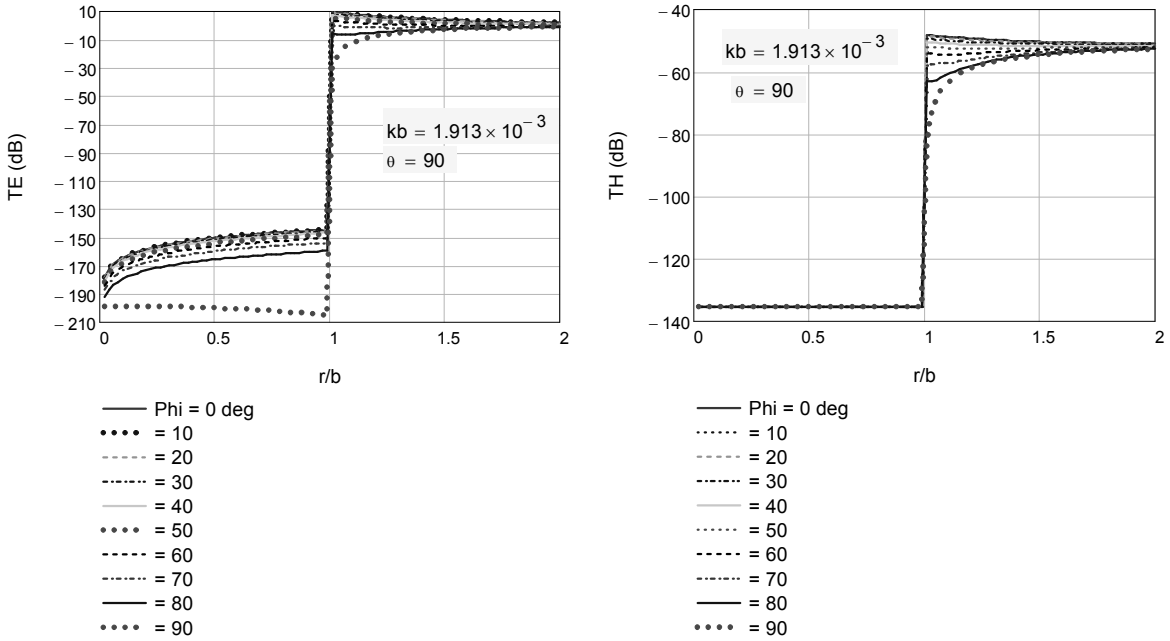

a. Electric field b. Magnetic field

Figure 5. Plots of the total E- and H-field transfer functions in the equatorial (z = 0) plane along different trajectories defined by the angle ϕ. (Parameters are b = 0.914 m, Δ = 0.794 mm, and f = 100 kHz.)

Another way of visualizing the EM field distribution in and around the shell it to plot the total field transfer function as a contour plot. This is done in Figure 6 for TE and in Figure 7 for TH. In these figures we see that for all practical purposes, the H-field is uniform within the shell. However, this is not the case for the E-field transfer function, where the TE at the center is considerably smaller than that elsewhere in the shell.

The frequency dependence of the solutions for the E-and H-fields of the shell are shown in Figure 8 over a frequency range from 100 kHz to 10 MHz. As this is a range of relatively low frequencies for the ~ 1 meter sphere size, we do not expect much of a change in the shape of the E-fields, but only a change in the E-field amplitudes within the shell. This is confirmed by the data in these plots. Clearly, as the frequency increases, the internal field strength is reduced, due to the inductive shielding provided by the currents flowing in the shell [22].

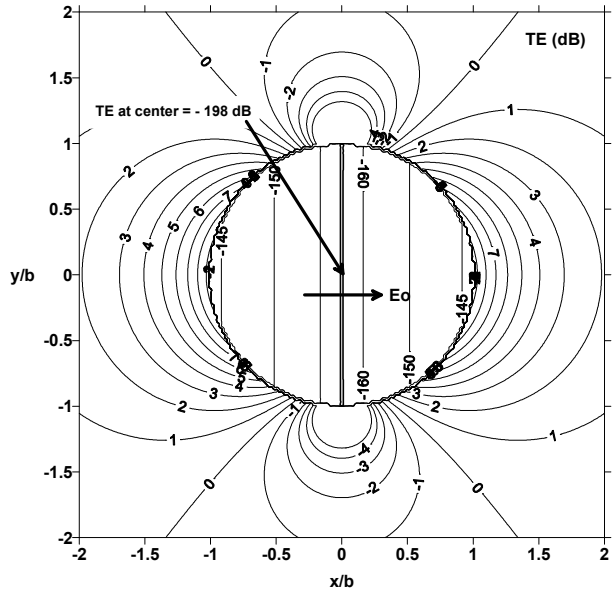

Figure 6. Contour plot of the total E-field transfer function (in dB)n the equatorial plane, inside and outside the aluminum shell, for b = 0.914 m, Δ = 0.794 mm, and f = 100 kHz.

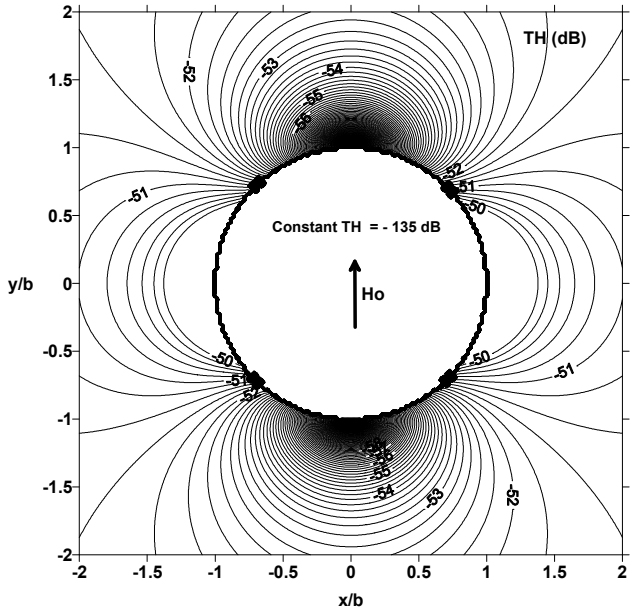

Figure 7. Contour plot of the total H-field transfer function (in dB) in the equatorial plane, inside and outside the aluminum shell, for b = 0.914 m, Δ = 0.794 mm, and f = 100 kHz.

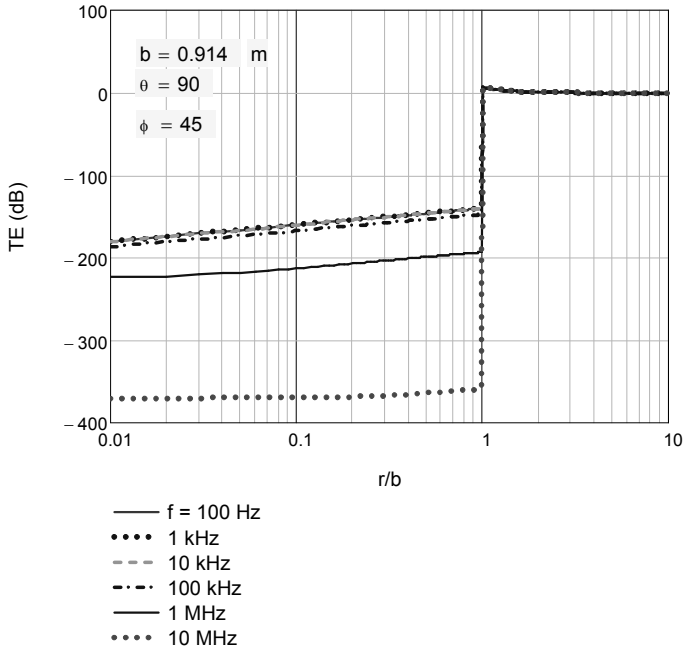

a. E-field transfer function

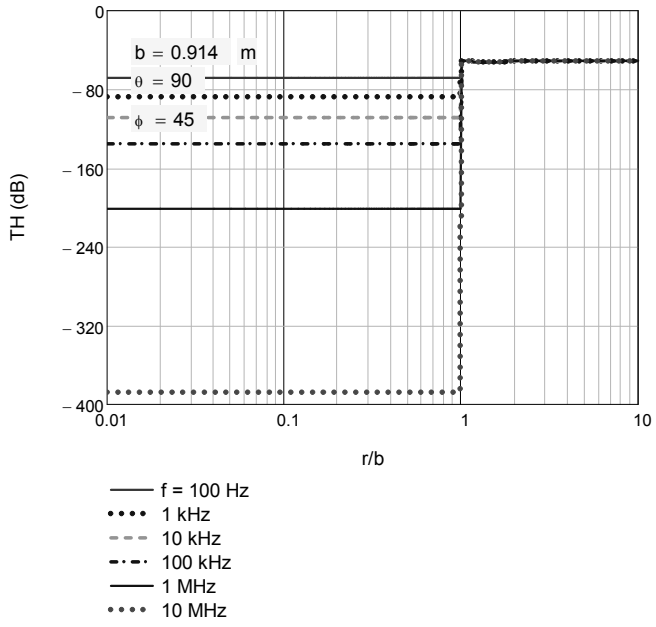

b. H-field transfer function

Figure 8. Illustration of the frequency dependence of the E- and H-field transfer functions, along a radial path defined by the angles $\theta = 90^{o}$ and $\phi = 45^{o}$ for the aluminum shell with $b = 0.914$ m and $\Delta = 0.794$ mm.

2.6 Statistical Description of the Internal Fields

To get a better quantitative description of the behavior of the EM fields within the spherical shell, Monte Carlo calculations were conducted for a wide range of frequencies on the aluminum shell (b = 0.914 m and Δ = 0.794 mm). In these simulations, the total E and H-fields at about 1000 randomly selected points within the shell were calculated and the response amplitudes were binned into histograms representing probability density functions. As an example, Figure 9 presents the histograms for the E-fields, computed at a frequency of 100 MHz. Clearly the H-field is a constant within the sphere, but the E-field has a wide range of values.

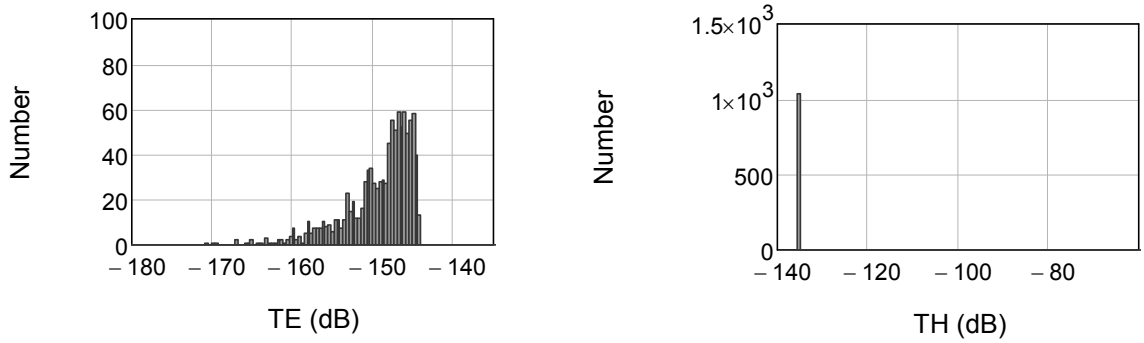

Figure 9. Example of the histogram functions for the internal E and H-fields for the aluminum sphere, at a frequency of 100 MHz.

From the histogram distributions, cumulative probability distributions (CPDs) can be calculated. Such distributions for the E-field are shown in Figure 10. These distributions represent the probability of a randomly selected point in the shell having a TE *less than* the value specified on the x-axis.

As seen in this figure, at very low frequencies (from 100 Hz to 10 KHz), the E-field CPDs are virtual overlays. At higher frequencies, the shielding begins to improve and the average values of the shielding becomes larger, with slight changes in the shape of the distributions.

As expected, the H-field CPDs are much less interesting, due to the almost uniform nature of the internal H-field in the shell. Figure 11 presents these results, where there is a slight hint of a change in the slope of the CPD at high frequencies.

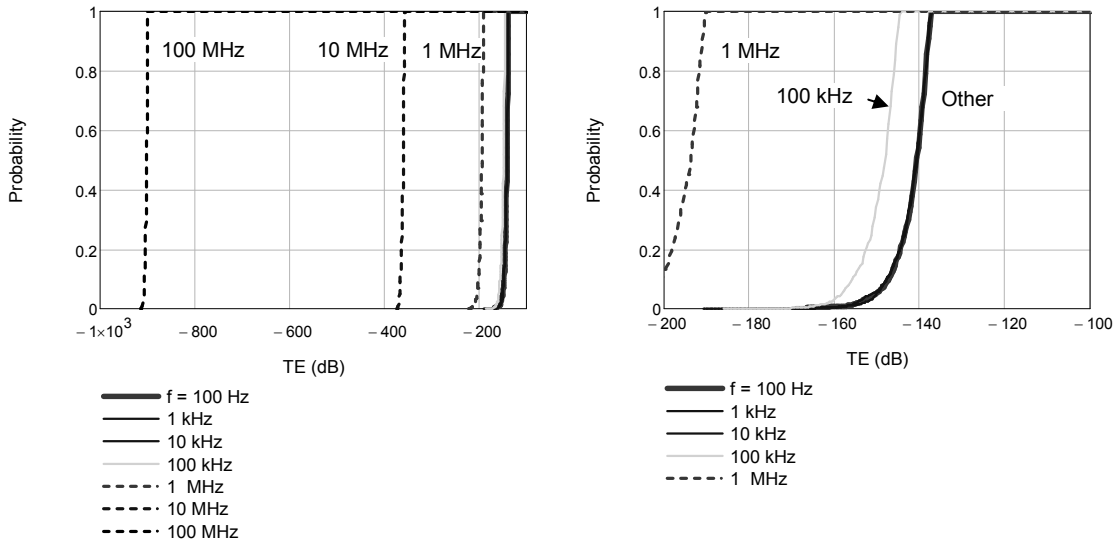

a. Complete frequencies range b. Low frequency range

Figure 10. Cumulative probability distributions for the E-field within the aluminum shell (b = 0.914 m and Δ = 0.794 mm), shown for various frequencies.

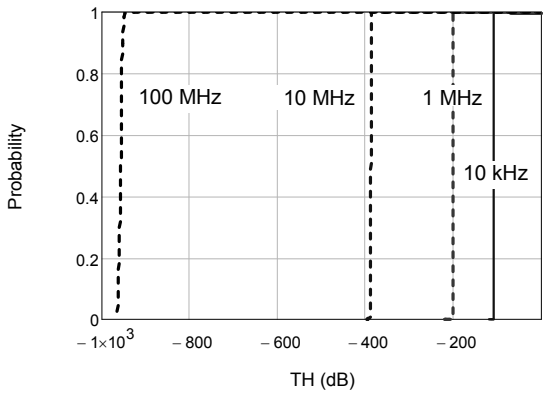

Figure 11. Cumulative probability distributions for the H-field within the aluminum shell, shown for various frequencies.

One way of summarizing the distributions of the internal field is by the mean value and standard deviation of the histograms. These quantities have been computed for the aluminum shell and are listed in Table 2. In addition to the data computed for the E-fields within the entire shell volume, the shielding values for the E-field and H-field at the center of the sphere from [8] are also listed.

From this summary, it is clear that the use of the H-field at the center of the shell as a representative sample of the shielding anywhere in the shell is a good measure. However, the same is not the case for the E-field at low frequencies, say below 1 MHz.

Table 2. Summary of the mean values and standard deviations of the distributions computed for the internal E- and H-fields of the aluminum shell.

Case	Frequency (Hz)	Avg. TE (dB)	TE Std. Dev. (dB)	TE (dB) from Ref.[8]	Avg. TH (dB)	TH Std. Dev. (dB)	TH (dB) from Ref.[8]
1	1.0E+02	-142	4.3	-251	-68	0.1	-68
2	1.0E+03	-142	4.2	-231	-88	0.1	-88
3	1.0E+04	-142	4.4	-211	-108	0.0	-108
4	1.0E+05	-149	4.4	-199	-135	0.0	-135
5	1.0E+06	-195	4.7	-224	-201	0.1	-201
6	1.0E+07	-360	3.1	-370	-388	0.4	-387
7	1.0E+08	-902	2.3	-900	-956	3.8	-958

3. Summary

This part of the paper has examined a simple canonical shielding problem with the goal of trying to gain a better understanding of the EM shielding provided by real shielding enclosures. The shield considered here was a spherical shell – one being made of finitely conducting material (aluminum) and having a finite wall thickness.

The reason for choosing this simple shape was that the calculation of the internal fields could be done mathematically through the use of spherical harmonics. This provides the possibility of evaluating the E- and H-fields anywhere inside or outside the sphere. In developing this analysis, closed form expressions for the expansion coefficients have been found, and these do not appear to be generally available in the literature. Moreover, a unique scaling technique was introduced that permits the accurate evaluation of the spherical Hankel function terms of the wave functions. This scaling is not an approximation to the Hankel functions as obtained by [11] and others, but is exact.

The benefit of this type of solution is that a Monte Carlo simulation can be used to develop probability distributions for the internal fields that show the variability of the field magnitudes. The difficulty, however, is that the solution is in the form of an infinite series of factors, which, at times, is difficult to sum. Moreover, there are numerical challenges in calculating the required Hankel functions of complex argument inside the lossy material due to numerical overflow and underflow.

This paper will conclude with Part 2, which deals with the quasi-static analysis of a spherical shell having an aperture.

4. References

1. "IEEE Standard Method for Measuring the Effectiveness of Electromagnetic Shielding Enclosures", IEEE STD 299-1997, 9 December 1997.
2. "High-Altitude Electromagnetic Pulse (HEMP) Protection for Ground-Based C4I Facilities Performing Critical, Time-Urgent Missions", MIL-STD-188-125-1, 17 July 1998.
3. IEC-61000-5-6, Electromagnetic Compatibility, Part 5: Mitigation Methods and Installation Guidelines, Section 6: Mitigation of External Influences, 2002-06.
4. Lee, K. S. H., ed., **EMP Interaction: Principles, Techniques and Reference Data**, Hemisphere Publishing Co. New York, 1989.
5. Lee, K. S. H., and G. Bedrosian, "Diffusive Electromagnetic Penetration into Metallic Enclosures", *IEEE Trans AP*, Vol. AP-27, No. 2, March 1979.
6. Kunz, K. S. and R. J. Luebbers, **The Finite Difference Time Domain Method for Electromagnetics**, CRC Press, Boca Raton, FL, 1993.
7. Stratton, J. A., **Electromagnetic Theory**, McGraw-Hill Book Co., New York, 1941.
8. Harrison, C. W. and C. H. Papas, "On the Attenuation of Transient Fields by Imperfectly Conducting Spherical Shells", *IEEE Trans AP*, Vol. AP-18, No 6, Nov. 1965.
9 Lindell, I. V., "Minimum Attenuation of Spherical Shields", *IEEE Trans AP*, Vol. AP-16, pp. 369-371, May 1968.
10 Shastry, S. V. K., K. N. Shamanna, and V. R. Katti, "Shielding of Electromagnetic Fields of Current Sources by Hemispherical Enclosures", *IEEE Trans AP,* Vol. EMC-27, No. 4, November 1985.
11. Baum C. E., "The Boundary-Connection Supermatrix for Uniform Isotropic Walls", *Interaction Notes*, Note 562, Air Force Research laboratory Directed Energy Directorate, 22 October 2000.

12. Franceschetti, G., "Fundamentals of Steady State and Transient Electromagnetic Fields in Shielding Enclosures," *IEEE Trans. EMC*, Vol. EMC-21, 1979.

13 Chang, S., "Scattering by a Spherical Shell with a Circular Aperture", University of Michigan technical report 5548-T-RL-2069, January 1968.

14. Ziolkowski, R. D. P. Marsland. L. F. Libelo and G.E. Pisane, "Scattering from an Open Spherical Shell Having a Circular Aperture and Enclosing a Concentric Dielectric Sphere", *IEEE Trans AP*., Vol. 36, No. 7, July 1988.

15. Enander, B., "Scattering by a Spherical Shell With a Small Circular Aperture", *EMP Interaction Notes*, Note 77, August 1971.

16. Sancer, M. I, and N. A. Varvatsis, "Electromagnetic Penetrability of Perfectly Conducting Bodies Containing an Aperture", *EMP Interaction Notes*, Note 49, August 1970.

17. Casey, K. F., "Quasi-Static Electric- and Magnetic-Field Penetration of a Spherical Shield Through a Circular Aperture", *IEEE Trans EMC*, Vol. EMC-27, No. 1, February 1985.

18. Senior, T. B. A., and G. Desjardins, "Electromagnetic Field Penetration into a Spherical Cavity", *IEEE Trans EMC*, Vol. EMC-16, No. 4, November 1974.

19. Abramowitz, M. and I. A. Stegun, **Handbook of Mathematical Functions,** U.S. National Bureau of Standards, Washington, DC 1964.

20. Personal conversation with Prof. Chalmers Butler, ECE Department, Clemson University, May 2008.

21. Harrington, R. F., **Time Harmonic Electromagnetic Fields**, McGraw-Hill Book Co., New York, 1961.

22. Hoburg, J. F., "Principles of Quasi-static Magnetic Shielding with Cylindrical and Spherical Shields", *IEEE Trans. EMC*, Vol. 37, No. 4, November 1995.